On multiple-path sonic anemometer measurement theory

A. Cuerva, A. Sanz-Andrés, J. Navarro

List of symbols

a_{jr} components of matrix [A]
c sound speed, m/s
C_d dimensionless wave number associated with distances between path midpoints
C_l dimensionless wave number associated with path length
c_{xy}^{XY} components of matrix $[\mathbf{C}^{XY}]$; $XY \equiv AW, PA, PW, WP$; $xy \equiv aj, sa, sj, js$
$[\mathbf{C}^{AW}]$ anemometer system–wind system transformation matrix
$[\mathbf{C}^{PW}]$ See Eqs. (11) and (33)
$\mathrm{d}\mathbf{k}_{\perp}$ $\mathrm{d}k_{W2}\ \mathrm{d}k_{W3}$, m^{-2}
$\mathrm{d}p$ differential displacement of a pulse along a generic acoustic path, m
$\{\mathbf{d}\Psi\}$ vector configured by three orthogonal increments $\mathrm{d}\psi_j$ (j=1,2,3), m/s
$\mathbf{e}_{\mathbf{A}a}$ vectors defining the anemometer system (a=1,2,3)
$\mathbf{e}_{\mathbf{P}s}$ unit path vector; this vector defines the direction of an acoustic path (s=1,2,3)
$\mathbf{e}_{\mathbf{W}j}$ vectors defining the wind system (j=1,2,3)
$E(k)$ turbulence three-dimensional energy spectrum, $\mathrm{m}^3/\mathrm{s}^{-2}$
f frequency of turbulent wind speed, Hz
f_0 effective data delivering frequency, Hz

$$U_p^i(t) = \begin{bmatrix} 1 & 0 & 0 & 0 & 0 \\ 0 & 1 & 0 & 0 & 0 \\ 0 & 0 & 1 & 0 & 0 \\ 0 & 0 & 0 & 1 & 0 \\ 0 & 0 & 0 & 0 & 1 \end{bmatrix}$$

F_j dimensionless Lagrangian average of fluctuation velocity along path s, associated with the pulse travelling in direction ± (see Eq. (24))
F_{jt}^M spectral density function at one point, corresponding to fluctuation components jt of wind speed vector, $\mathrm{m}^3/\mathrm{s}^2$
g measured spectral density function at one point, corresponding to fluctuation components jt of wind speed vector, $\mathrm{m}^3/\mathrm{s}^2$
$G_s^{\pm}$ acceleration of gravity vector, m/s^2
$\mathbf{k}$ function defined by Eq. 31
k_{Wj} wave number vector, m^{-1}
j component of wave number vector expressed in the wind system, m^{-1}

k_{Aa} *a* component of wave number vector expressed in the anemometer system, m^{-1}

$\mathbf{k}_{\perp}$ $\{k_{W2},k_{W3}\}$, m^{-1}

l acoustic path length, m

$\mathbf{l}_{Ps}$ acoustic path vector (direction and modulus of acoustic path *s*, direction+coincident with the direction of the first firing), m

l_{Ps} length of acoustic path *s*, m

l_w representative length scale of wind speed variations associated with shear, surface blockage or thermal effects, m

M_{∞} Mach number of atmospheric flow related to mean wind speed vector modulus $|\mathbf{u}_{\infty}|$

MUSA 1 METEK USA 1 sonic anemometer model

n_0 number of measurements averaged in a final output

p pulse position on the acoustic path related to path origin, m

$p_{0s}^{\pm}$ acoustic path extremes of a generic path *s*, m

P dimensionless pulse position on the acoustic path related to path origin

$P_0^{\pm}$ dimensionless acoustic path extremes of a generic path *s*

q_{sj} see Eq. (35)

Q_s $0.5(G^+{}_s+G^-{}_s)$

R_{jt} ratio of measured spectral density function $F^{M}{}_{jt}$ and the theoretical spectral density function F_{jt} (in this paper, this ratio is referred to as "relation of spectral components")

ARS anemometer reference system

PRS path reference system

WRS wind reference system

t time, s

$t_s^{\pm}$ time required by an ultrasound pulse front to cover the distance $p_{0s}{}^{+}$ to $p_{0s}{}^{-}$ (case +) and $p_{0s}{}^{-}$ to $p_{0s}{}^{+}$ (case –) of a generic acoustic path *s*, s

$T_s^{\pm}$ dimensionless time required by an ultrasound pulse front to cover the distance $P_{0s}{}^{+}$ to $P_{0s}{}^{-}$ (case +) and $P_{0s}{}^{-}$ to $P_{0s}{}^{+}$ (case –) of a generic acoustic path *s*, s

$T_{0s}^{\pm}(P)$ zero-order estimation of dimensionless time required by an ultrasound acoustic pulse front travelling on the acoustic path *s* in direction ± to get at point *P*

$T_{1s}^{\pm}(P)$ first-order estimation of dimensionless time required by an ultrasound acoustic pulse front travelling on the acoustic path *s* in direction ± to get at point *P*

$\mathbf{u}(\mathbf{x}, t)$ atmospheric turbulent speed field, m/s

u_{Ps} component of wind speed vector parallel to path *s*, m/s

u_{wj} components of wind speed vector expressed in the wind system, m/s

$\bar{\mathbf{u}}$ mean wind speed vector, m/s

$\mathbf{u}^{\mathbf{M}}$ measured wind speed vector, m/s

u_{Wj}^{M} components of measured wind speed vector expressed in the wind system, m/s

$\mathbf{u}_{\mathbf{S}}^{\mathbf{M}}, \mathbf{u}_{\mathbf{P}}^{\mathbf{M}}$ vector formed by components of wind speed vector measured along each acoustic path *s*, m/s

u_S^M, u_p^M measurement of the wind speed vector component parallel to a generic acoustic path *s*, m/s

$\hat{\mathbf{u}}_{Wj}$ fluctuation components of the wind speed vector expressed in the wind system, m/s

$\hat{\mathbf{u}}$ wind speed fluctuation vector, m/s

$\hat{\mathbf{u}}^{\mathbf{M}}$ measured wind speed fluctuation vector, m/s

U_{Ps} dimensionless speed component along a generic acoustic path *s*

U_{Ps}^{M} dimensionless measured speed component along a generic acoustic path *s*

$U_{Wjs}^{\pm}$ dimensionless component of wind speed vector at the ultrasound pulse location (time and point) travelling on the generic acoustic path s in direction ±, respectively

$\hat{U}_{Wjs}^{\pm}$ fluctuation component of $U_{Wjs}^{\pm}$

$\mathbf{x}$ location where the wind speed vector is evaluated, m

$\mathbf{x}_{\mathbf{P}}$ geometric center of path midpoints, m

$\mathbf{x}_{\mathbf{A}}$ anemometer system origin, m

$\mathbf{x}_{\mathbf{P}s}$ midpoint of path *s*, m

$(\mathbf{x}_{\mathbf{A}},\mathbf{e}_{\mathbf{A}a})$ anemometer system, m

$(\mathbf{x},\mathbf{e}_{\mathbf{W}j})$ wind system, m

$(\mathbf{x}_{\mathbf{P}},\mathbf{e}_{\mathbf{P}s})$ PRS, m

x_{Pasa} co-ordinates of the midpoint of a generic acoustic path *s* expressed in the anemometer system, m

$\mathbf{X}$ location where the wind speed vector is evaluated, dimensionless

$\mathbf{X}_{\mathbf{P}s}$ dimensionless midpoint of path *s*

z_B time delay between two consecutive pulse firings, s

Z_B dimensionless time delay between two consecutive pulse firings

α angle formed by mean wind speed vector and the bisect of the angle formed by the two acoustic paths in Kaimal's problem, see Fig. 3, rad

α_E energy spectrum constant

ε scale factor of fluctuation speed

$\in$ viscous dissipation rate of turbulent kinetic energy, m^2/s^3

γ_{As} angle formed by a generic acoustic path *s* and the plane $\mathbf{e}_{\mathbf{A1}}$–$\mathbf{e}_{\mathbf{A2}}$, rad

γ_{AW} Elevation angle of the mean wind speed vector in the anemometer system, rad

η Kolmogorofs length, m

$[\Phi]$ spectral velocity tensor, m^5s^{-2}

$\Phi_{jt}(\mathbf{k})$ component of the spectral velocity tensor, m^5/s^2

$[\Phi]^M$ measured spectral velocity tensor, m^5/s^2

$\Phi_{jt}^{M}(\mathbf{k})$ measured *jt* component of the spectral velocity tensor, m^5/s^2

λ l_W/l *ratio*

θ_{As} angle between the projection of a generic acoustic path *s* on the plane $\mathbf{e}_{\mathbf{A1}}$–$\mathbf{e}_{\mathbf{A2}}$ and $\mathbf{e}_{\mathbf{A1}}$, rad

θ_{AW} azimuth angle of mean wind speed vector in the anemometer system, rad

θ half-angle formed by the two paths in the Kaimal's problem configuration (see Fig. 3), rad

$\Psi_j(\mathbf{k},t)$ function with orthogonal increments (homogeneous turbulence model) that define the theoretical fluctuation turbulent wind speed field (j=1,2,3), m/s

$\Psi M_j(\mathbf{k},t)$ function with orthogonal increments (homogeneous turbulence model) that define the measured fluctuation turbulent wind speed field (j=1,2,3), m/s

1 Introduction

Sonic anemometers along with cup, propeller and hot wire anemometers are sensors extensively used in atmospheric applications (Cuerva and Sanz-Andrés 2000; Kaimal 1978). More recently, this technology has been applied to wind engineering (Kato et al. 1992) and wind energy disciplines (Cuerva 2001; Cuerva and Sanz-Andrés 1999).

Sonic anemometers present some advantages over the other technologies cited above. First, sonic anemometers are able to measure the complete wind speed vector, whereas the other technologies cannot or need to use three sensors. Secondly, a sonic anemometer is especially robust and is the only type of sensor that simply requires an initial calibration, which is a clear advantage in harmful environments like the atmosphere. Finally, a sonic anemometer can reach useful sampling rates to the order of 100 Hz, much larger than the corresponding cup anemometer (Cuerva and Sanz-Andrés 1999, 2000).

The measuring principle of sonic anemometers can be implemented in several ways (Cuerva 2001). The most extended methodology is based on pulsed signals and in the algorithm of inverses of travel times.

$$u_{Ps}^{M} = \frac{l}{2}\left(\frac{1}{t_s^-} - \frac{1}{t_s^+}\right) \tag{1}$$

where l is the length of the acoustic path, and $t_s^{\pm}$ is the time required by the pulses to cover the distance between transducers in sense + and – respectively. This algorithm allows estimates of the measured flow speed component along the acoustic path, once the pulse has covered the distance between transducers in both senses.

A three-path sonic anemometer requires six pulses to estimate one value of the wind speed vector. A time delay between consecutive shots of pulses, z_B, exists. Also, some additional time at the end of the sequence is needed by the sensor control to carry out calculations and resetting of electronics. Hence, a complete measuring sequence normally lasts for a time slightly larger than $6z_B$.

The measured values corresponding to a single sequence can be given directly by the sensor, therefore at an equivalent sampling rate $f_0=(6z_B)^{-1}$ or block averaged in n_0 groups, resulting in a lesser effective sampling rate $f_0=(n_0 6z_B)^{-1}$.

Sonic anemometers show two types of errors. The first class are directional errors associated with the measurement of mean values of wind speed vector. These errors are due to aerodynamic interference of the sensor's structure (Cuerva and Sanz-Andrés 1999). The second type are also directional errors but associated with the measurement of turbulent characteristics. These characteristics make these sensors behave as directional filters, which attenuate or amplify the measurement of spectral density functions, depending on the angles of incidence of wind speed vector, among other parameters (Cuerva and Sanz-Andrés 1999). The measuring process of sonic anemometers itself gives rise to this second type of errors (Cuerva and Sanz-Andrés 2000; Kaimal et al. 1968).

Sonic anemometer modeling can be split into two general parts. The first one deals with the model of one measurement sequence (Cuerva and Sanz-Andrés 2000) and the second one deals with the modeling of the discrete process of sampling and averaging of n_0 single sequence blocks (Kaimal 1978; Cuerva 2001; Henjes et al. 1999). Both sub-processes have an important influence in the measurement of the wind speed vector. In this paper, only the model of a single sequence is presented. Therefore, the results shown in this work are the first part of a total model of the complete sonic measuring process.

The model is based on a description, by means of basic cinematic equations, of the travel of pulses between the transmitter and receiver of the acoustic paths that configure sonic anemometers (Cuerva and Sanz-Andrés 2000). The wind speed field is assumed to change during the pulse travel time and during the time delays between the pulses shots that configure a measuring sequence. This hypothesis was already applied by the authors to a one-path sonic model (Cuerva and Sanz-Andrés 2000). The main hypothesis of this work is that this change of the wind speed field affects the measurement.

Three simplifications are applied in this work. The first simplification is to consider that the travel of one pulse along the acoustic path is only affected by the local component of wind speed vector that is parallel to the acoustic path. This simplification leads to an error of order M_∞^2 (M_∞ is the Mach number of the flow associated with the module of the mean wind speed vector, $|u_\infty|$, for a steady and uniform flow field case (Kaimal 1978), and to errors of order εM_∞ for a general non-steady and non-uniform case (Cuerva and Sanz-Andrés 2000) (ε is the order of magnitude of the wind speed perturbation).

The second simplification consists of considering a model of incompressible homogeneous and isotropic turbulence.

Incompressible turbulence simplification implies Mach numbers $M_\infty << 1$. However, some computational experiments are presented in this work for M_∞=0.2 and M_∞=0.4. These values are clearly beyond the compressibility threshold. This fact would imply the use of a compressible turbulence model. The Mach number is fundamentally used here to quantify the importance of

mean flow speed related to sound speed in the transmission of pulses, instead of quantifying compressibility effects. In normal atmospheric applications of sonic anemometers the Mach number is $M_\infty << 1$. The values $M_\infty > 0.1$ should be understood as a test for the limits of applicability of the developed sonic anemometer model.

The usual expression for wind speed vector, defined as a summation of an averaged component of several realizations, u_∞, plus three fluctuation components, $\hat{u}_{wj}$, j=1,2,3, with zero mean value is considered:

$$\mathbf{u}(\mathbf{x},t) = \{[|\mathbf{u}_\infty| + \hat{u}_{W1}(\mathbf{x},t)] + \hat{u}_{W2}(\mathbf{x},t) + \hat{u}_{W3}(\mathbf{x},t)\} \tag{2}$$

The previously cited assumption of homogeneity (Batchelor 1952) allows the use of a Fourier–Stieldges expression for the fluctuation components of wind speed vector as follows:

$$\hat{u}_{Wj}(\mathbf{x},t) = \int_{-\infty}^{\infty} \mathrm{e}^{i\mathbf{k}\mathbf{x}} d\Psi_j(\mathbf{k},t) \tag{3}$$

where $\mathbf{k}$ is the wavenumber vector, $\mathbf{x}$ is the point where the fluctuation components of wind speed vector are being evaluated, and $\mathrm{d}\Psi_j(\mathbf{k}, t)$ are orthogonal increments of proper random functions which are not correlated due to the homogeneity assumption. On the other hand, the spectral velocity tensor can be expressed in terms of these increments. Both facts are expressed as follows (Kaimal 1978; Batchelor 1952):

$$\overline{d\Psi_j(\mathbf{k},t) d\Psi_t^*(\mathbf{k}',t)} = \begin{cases} 0, \mathbf{k} \neq \mathbf{k}' \\ \Phi_{jt}(\mathbf{k})\mathrm{d}\mathbf{k}, \mathbf{k} = \mathbf{k}' \end{cases} \tag{4}$$

The expression used in this work for the isotropic spectral velocity tensor, Φ_{jt} is given by (Kaimal et al. 1968; Mann 1994):

$$\Phi_{jt}(\mathbf{k}) = \frac{E(k)}{4\pi k}\left(k^2\delta_{jt} - k_j k_t\right) \tag{5}$$

where $E(k)$ is the energy spectrum function. In this work, the Von Kármán expression for $E(k)$ is used (Von Kármán 1958):

$$E(k) = \alpha_E \in^{\frac{2}{3}} l_W^{\frac{5}{3}} \frac{(l_W k)^4}{\left[1 + (l_W k)^2\right]^{\frac{17}{6}}} \tag{6}$$

where $\in$ is the viscous dissipation ratio of turbulent kinetic energy, l_W is a characteristic flow length scale associated with energy transference phenomena such as surface eddy blocking or vertical shear, and α_E is an empirical value.

Homogeneity and isotropy simplifications do not allow the consideration of certain real effects such as vertical shear or surface blockage of wind speed. Isotropy does not allow any direct conclusion on cross-spectra to be obtained, since isotropy forces spectral density functions F_{jt} (jt=12, 13, or 23) to be zero.

The third simplification is to consider the validity of Taylor's hypothesis of frozen turbulence. This hypothesis allows wind speed to be obtained at a specific point x in time t from wind speed at point x–u_∞ t at t=0 s.

In Sect. 2, the mathematical model of the three-paths sonic anemometer speed vector build-up process from the single-path measured velocity components is presented in.In Sect. 3, the model of the sonic pulse travel time in a non-steady, non-uniform flow field is introduced, and solved for the case of an incompressible, isotropic turbulent flow (Sects. 4 and 5).

The results are employed to compare the ratio of measured to theoretical spectral density functions, and to analyze the influence of the parameters involved (Mach number, delay between consecutive pulses, wind direction, inclination of mean wind speed vector, etc.) for both two-path and three-path sonic anemometers (Sects. 6, 7, and

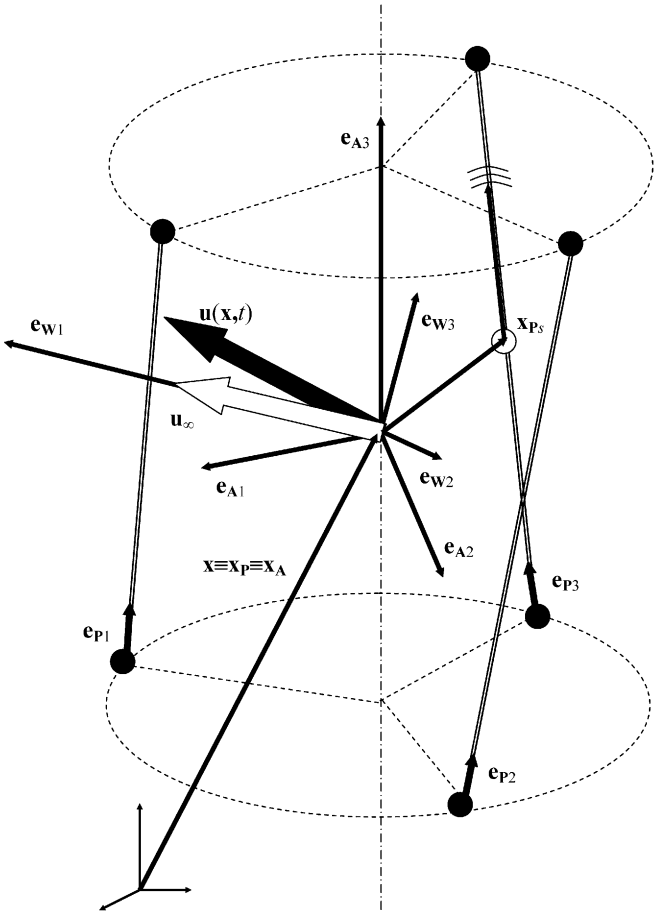

Fig. 1. Basic geometry of a three-path sonic anemometer and representation of the different reference systems. The emitter–receiver pair that defines each acoustic path is represented by black dots: ($\mathbf{x}_A$, $\mathbf{e}_{Aa}$), Anemometer system; ($\mathbf{x}$, $\mathbf{e}_{Wj}$), Wind system; $\mathbf{e}_{Ps}$, path s direction

8). Also, new limits for the frequency range of undistorted frequency response are determined for these specific sonic anemometer configurations. These new limits are compared with Kaimal's limits.

2 Three-path sonic anemometer

In order to clarify the mathematical model development, the process is outlined as follows: The components of the wind speed vector $\mathbf{u}(\mathbf{x},t)$ along each of the acoustic paths of a sonic anemometer, u_{Ps}, are calculated in the first step. The components of measured wind speed vector along the acoustic paths, $u^{M}{}_{Ps}$, are then obtained. Finally, the measured wind speed vector, $\mathbf{u}^{\mathbf{M}}(\mathbf{x},t)$, is expressed in an adequate reference system.

To carry out this process, two reference systems are defined. The first one is the wind reference system (Wind system). The Wind system is represented by ($\mathbf{x}$, $\mathbf{e}_{Wj}$), j=1,2,3; where $\mathbf{x}$ is the point of the space that the measure of the wind speed vector is related to, $\mathbf{e}_{W1}$ is aligned with the mean wind speed vector, $\mathbf{u}_{\infty}$; $\mathbf{e}_{W3}$ is orthogonal to $\mathbf{e}_{W1}$, and it points to $-g$ half-space, g being the gravity acceleration vector; and finally $\mathbf{e}_{W2}$ is chosen to define the Wind system as a right-hand orthonormal reference system (see Fig. 1). In the Wind system, the wind speed vector presents its simplest expression, previously referred in the Introduction.

A second reference system, named the anemometer reference system (Anemometer system), is in the calculation of the wind speed vector projections along the acoustic paths and, afterwards, the calculation of the measured wind speed vector expressed in the Wind system. The Anemometer system is represented by ($\mathbf{x}$, $\mathbf{e}_{Aa}$), a=1,2,3, where $\mathbf{x}_A$ is the point of the anemometer where the measured values are referred to, $\mathbf{e}_{Aa}$ are three orthonormal vectors oriented along the three nominal directions employed by the anemometer as the reference for the three measured speed components (see Fig. 1). The Anemometer system is a right-hand reference system.

In a general case, the origins of the Wind system and the Anemometer system, $\mathbf{x}$ and $\mathbf{x}_A$ respectively, do not coincide, as is the case in Fig. 1. However, without losing general application, it is convenient to make those origins coincide, $\mathbf{x}=\mathbf{x}_A$; so that a common reference for the real wind speed vector, $\mathbf{u}(\mathbf{x},t)$, and the measured one, $\mathbf{u}^{\mathbf{M}}(\mathbf{x},t)$, is obtained.

Each of the acoustic paths is identified in Fig. 1 by the unit vectors $\mathbf{e}_{Ps}$, s=1,2,3. The components of $\mathbf{u}(\mathbf{x},t)$ along each acoustic path, $\mathbf{e}_{Ps}$, are obtained

$$u_{Ps}(\mathbf{x},t) = \mathbf{u}(\mathbf{x},t)\mathbf{e}_{Ps} \tag{7}$$

and the vectors $\mathbf{u}(\mathbf{x},t)$ and $\mathbf{e}_{Ps}$ should be written in the same reference system. In this case, the Anemometer system is selected for convenience.

Let us introduce some definitions. In the Anemometer system, each acoustic path is defined by its midpoint, $\mathbf{x}_{Ps}$, and the product $l_{Ps}\,\mathbf{e}_{Ps}$, where the scalar l_{Ps} is the length of the acoustic path s. As shown in Fig. 2, the vectors $\mathbf{e}_{Ps}$ form an angle γ_{As} with the plane ($\mathbf{e}_{A1}$,$\mathbf{e}_{A2}$). The projection of $\mathbf{e}_{Ps}$ on this plane ($\mathbf{e}_{A1}$,$\mathbf{e}_{A2}$) forms an angle θ_{As} with $\mathbf{e}_{A1}$ axis. In all these cases, s=1,2,3.

In general, it is convenient to make $\mathbf{x}=\mathbf{x}_{\mathbf{A}}=\mathbf{x}_{\mathbf{P}}$, $\mathbf{x}_{\mathbf{P}}$ being the geometric center of the midpoints of the acoustic paths, $\mathbf{x}_{Ps}$. Therefore, the real wind speed vector, $\mathbf{u}(\mathbf{x},t)$, and the measured one, $\mathbf{u}^{\mathbf{M}}(\mathbf{x},t)$ are associated with a common point with physical relevance in the sensor. From now on, this point will be referred to as $\mathbf{x}$.

Considering the previous definitions, each vector $\mathbf{e}_{Ps}$ is expressed in the Anemometer system by the co-ordinates c_{sa}^{PA}, as indicated in Eq. (8).

$$\mathbf{e}_{Ps}\big|_{\mathrm{ARS}} = \{\cos\theta_{As}\cos\gamma_{As}, \sin\theta_{As}\cos\gamma_{As}, \sin\gamma_{As}\} = \{c_{sa}^{PA}\} \tag{8}$$

The transformation matrix between the Wind system and the Anemometer system, $[\mathrm{C}^{AW}]$ is given by

$$[\mathbf{C}^{AW}] = \begin{bmatrix} \cos\theta_{AW}\cos\gamma_{AW} & -\sin\theta_{AW} & -\cos\theta_{AW}\sin\gamma_{AW} \\ \sin\theta_{AW}\cos\gamma_{AW} & \cos\theta_{AW} & -\sin\theta_{AW}\sin\gamma_{AW} \\ \sin\gamma_{AW} & 0 & \cos\gamma_{AW} \end{bmatrix} \tag{9}$$

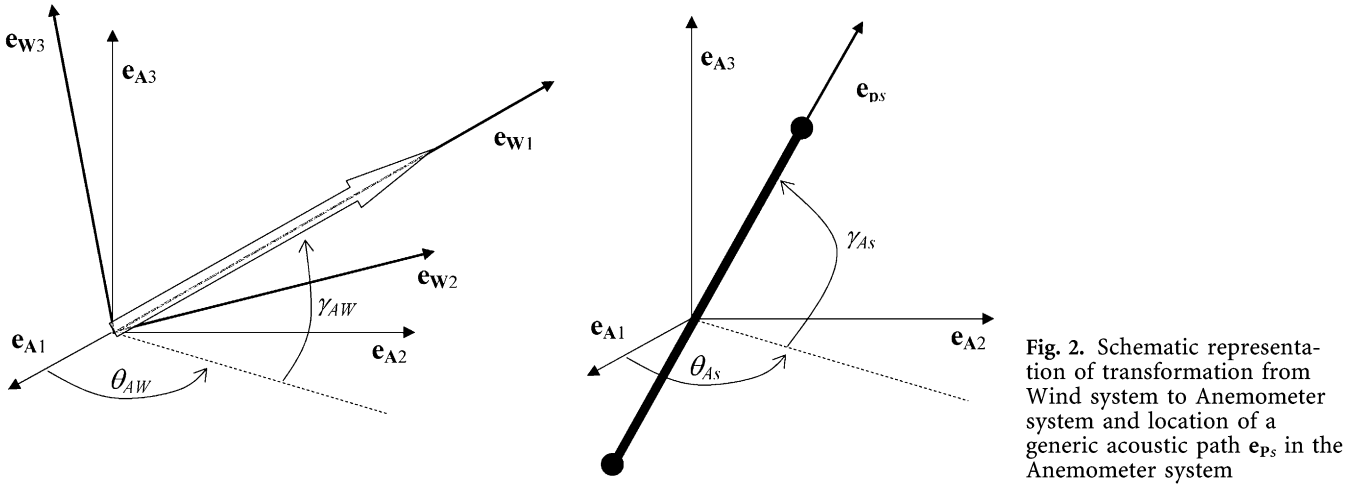

Fig. 2. Schematic representation of transformation from Wind system to Anemometer system and location of a generic acoustic path $\mathbf{e}_{Ps}$ in the Anemometer system

The matrix $[C^{AW}]$ allows us to obtain the expression of vector $\mathbf{u}(\mathbf{x},t)$ in the Anemometer system from its components in the Wind system.

$$\mathbf{u}(\mathbf{x},t)|_{\mathrm{ARS}} = [\mathrm{C_{AW}}]\mathrm{u}(\mathrm{x},t)|_{\mathrm{WRS}} = \{u_{aj}\} \tag{10}$$

Using Eqs. (8) and (10), the dot product in Eq. (7) finally gives rise to

$$\begin{aligned} u_{Ps} &= \mathbf{u}(\mathbf{x},t)|_{\mathrm{ARS}}\mathbf{e}_{\mathrm{Ps}}|_{\mathrm{ARS}} = \{u_a\}\{c_{sa}^{PA}\} = c_{aj}^{AW}c_{sa}^{PA}u_{wj} \\ &= c_{sj}^{PW}u_{wj} \end{aligned} \tag{11}$$

3
Pulse travel time

The model proposed by the authors in (Cuerva and Sanz-Andrés 2000) for one acoustic path, is applied to describe the travel of pulses along a generic path of a sensor with three acoustic paths. A generalization of the process followed in Cuerva and Sanz-Andrés (2000) is included here in order to clarify the presentation.

The travel times for pulses travelling in both directions, + and –, of the acoustic path $l_{Ps}\mathbf{e}_{Ps}$, are represented here by variables $t_s^{\pm}$.

$$t_s^{\pm} = \int_{P_{0s}^{\pm}}^{p_{0s}^{\mp}} \frac{\mathrm{d}p}{\pm c + u_{Ps}(p,t)} \tag{12}$$

where c is the sound speed in the fluid, $u_{Ps}(\mathrm{x},t)$, are the projections of vector $\mathbf{u}(\mathbf{x},t)$ along the acoustic path $\mathbf{e}_{Ps}$. In this case, such projections are evaluated in time t at a distance p, on the acoustic path $\mathbf{e}_{Ps}$, from the acoustic path extremes p_{0s}^{+} and p_{0s}^{-}. The problem represented in Eq. (12) is solved using dimensionless variables defined as follows:

$$T = t\frac{|\mathrm{u}_\infty|}{l},\ P = \frac{p}{l},\ M_\infty = \frac{|\mathrm{u}_\infty|}{c},\ U = \frac{u}{|\mathrm{u}_\infty|},\ \widehat{U}_{Wj} = \frac{\widehat{u}_{Wj}}{|\mathrm{u}_\infty|}, \tag{13}$$

where T, P, and U are the dimensionless time, position on the path and wind speed, respectively; M_∞ is the Mach number based on the module of the mean wind speed vector, $\mathbf{u}_\infty$, and l is the characteristic length of the problem that coincides with the lengths of the acoustic paths if these are the same for the three paths.

Then, in dimensionless form, Eq. (12) becomes

$$T_s^{\pm} = M_\infty \int_{P_{0s}^{\pm}}^{P_{0s}^{\mp}} \frac{\mathrm{d}P}{\pm 1 + \mathrm{M}_\infty U_{Ps}(P,T)} \tag{14}$$

If the real wind speed field, $\mathbf{u}(\mathbf{x},t)$, is known [therefore $u_{Ps}(\mathbf{x},t)$ and its dimensionless form $U_{Ps}(P,T)$], Eq. (1) allows to know the dimensionless measurement of the components U_{Ps}^{M} of wind speed vector, $\mathbf{u}(\mathbf{x},t)$.

$$U_{Ps}^{M} = \frac{l}{2|\mathbf{u}_\infty|}\Delta\left[\frac{1}{t}\right] = \frac{1}{2}\left[\frac{1}{T_s^{-}} - \frac{1}{T_s^{+}}\right] \tag{15}$$

4
Solution of the equations

The way the pulse travel equations were solved in (Cuerva and Sanz-Andrés 2000) for one path is generalized here for a generic acoustic path. The generalized expression corresponding to Eqs. (46) in Cuerva and Sanz-Andrés (2000) are the differential form of Eqs. (14).

$$\begin{aligned} &\mathrm{d}T_s^{\pm}(\mathbf{X},\mathbf{X}_{\mathrm{Ps}},T,P) = \pm\frac{\frac{M_\infty}{1\pm c_{sj}^{PW}M_\infty}\mathrm{d}P}{1 \pm \frac{M_\infty}{1\pm c_{s1}^{PW}M_\infty}c_{sj}^{PW}\widehat{U}_{Wj}(\mathbf{X},\mathbf{X}_{\mathrm{Ps}},P,T)}; \\ &T_s^{\pm}\left(\mathbf{X},\mathbf{X}_{\mathrm{Ps}},-\frac{1}{2}\right) = 0, T_s^{-};\ T_s^{\pm}\left(\mathbf{X},\mathbf{X}_{\mathrm{Ps}},\frac{1}{2}\right) = T_s^{+},0 \end{aligned} \tag{16}$$

where $\mathrm{d}T_s^{\pm}$ is the dimensionless time required by a pulse travelling in a sense ± to cover a distance $\mathrm{d}P$ along the acoustic path $\mathbf{e}_{Ps}$.

The problem defined in Eq. (16) is solved by applying a perturbation method equivalent to the one presented in Eq. (11) in Cuerva and Sanz-Andrés (2000),

$$T_s^{\pm}(P) \cong T_{0s}^{\pm}(P) + \varepsilon T_{1s}^{+}(P) \tag{17}$$

where $T_s^{\pm}$ is the zero-order time and $\varepsilon T_{1s}^{\pm}$ is the dimensionless time perturbation of order ε, being ε the order of magnitude of wind speed perturbation.

The use of expansion considered in Eq. (17) to the problem defined by Eq. (16) leads to

$$\begin{aligned} &\mathrm{d}T_{0s}^{\pm}(P) + \varepsilon\mathrm{d}T_{1s}^{\pm}(P) \\ &\quad = \pm\frac{M_\infty}{1 \pm c_{s1}^{PW}M_\infty}\left(1 \mp \frac{M_\infty}{1 \pm c_{s1}^{PW}M_\infty}c_{sj}^{PW}\widehat{U}_j(\mathrm{X},\mathrm{X}_{\mathrm{Ps}},P,T)\right) \\ &\qquad \times\ \mathrm{d}P + O\left(\varepsilon^2 M_\infty\right) \end{aligned} \tag{18}$$

Equation (18) can be split into two problems, one for each sense of pulse travel. The zero and first-order problems are, respectively

$$\mathrm{d}T_{0s}^{\pm}(P) = \pm\frac{M_\infty}{1 \pm c_{s1}^{PW}M_\infty}\mathrm{d}P,\ T_{0s}^{\pm}\left(\mp\frac{1}{2}\right) = 0 \tag{19}$$

$$\begin{aligned} \varepsilon\mathrm{d}T_{1s}^{\pm}(P) = &-\left[\frac{M_\infty}{1 \pm c_{s1}^{PW}M_\infty}\right]^2 \\ &\times\ \mathrm{c}_{\mathrm{sj}}^{\mathrm{PW}}\widehat{\mathrm{U}}_{\mathrm{j}}(\mathrm{X},\mathrm{X}_{\mathrm{Ps}},P,T)\mathrm{d}P;\ T_{1s}^{\pm}\left(\mp\frac{1}{2}\right) = 0 \end{aligned} \tag{20}$$

Equations (19) and (20) can be solved and the solutions are

$$T_{0s}^{\pm}(P) = \frac{M_\infty}{1 \pm c_{s1}^{PW}M_\infty}\left(\frac{1}{2} \pm P\right) \tag{21}$$

$$T_{s1}^{\pm}(P) = -\left[\frac{M_\infty}{1 \pm c_{s1}^{PW} M_\infty}\right]^2 \times \int_{\mp\frac{1}{2}}^{P} c_{sj}^{PW} \widehat{U}_{Wj}\left[\mathrm{X}, \mathrm{X}_{\mathrm{Ps}}, P, T_{0s}^{\pm}(P)\right] \mathrm{d}P \tag{22}$$

The total travel times for the ± pulses along the acoustic path $\mathbf{e}_{\mathbf{P}s}$ are

$$\begin{aligned} T_s^{\pm}\left(\mathbf{X}, \mathbf{X}_{\mathrm{Ps}}, \pm\frac{1}{2}\right) &\cong T_{0s}^{\pm}\left(\pm\frac{1}{2}\right) + \varepsilon T_{1s}^{\pm}\left(\mathbf{X}, \mathbf{X}_{\mathrm{Ps}}, \pm\frac{1}{2}\right) \\ &= T_s^{\pm}\left(\mathbf{X}, \mathbf{X}_{\mathrm{Ps}}, \pm\frac{1}{2}\right) \\ &= \frac{M_\infty}{1 \pm c_{s1}^{PW} M_\infty}\left(1 \mp \frac{M_\infty}{1 \pm c_{s1}^{PW} M_\infty} \varepsilon F_s^{\pm}(\mathbf{X}, \mathbf{X}_{\mathrm{Ps}})\right) \end{aligned} \tag{23}$$

where

$$\begin{aligned} &\varepsilon F_s^{\pm}\left(\mathbf{X}, \mathbf{X}_{\mathrm{Ps}}, c_{sj}^{PW}, M_\infty\right) \\ &= \int_{-\frac{1}{2}}^{\frac{1}{2}} c_{sj}^{PW} \hat{U}_{WJ}\left[\mathbf{X}, \mathbf{X}_{\mathrm{Ps}}, P, T_{0s}^{\pm}\left(P, c_{s1}^{PW}, M_\infty\right)\right] \mathrm{d}P \end{aligned} \tag{24}$$

between the firing of initial pulse of the sequence and a generic instant when a generic pulse reach a generic point of the corresponding acoustic path in a ± direction, is given by

$$T_{0s}^{\pm} = \left(2s - \frac{1}{2}(3 \pm 1)\right) Z_B \tag{27}$$

Equation (27) indicates that fluctuation speed components that are faced by a point of an ultrasound pulse front when it is located at point $\mathbf{x}+\mathbf{x}_{\mathbf{P}s}+l_{Ps}P\mathbf{e}_{\mathbf{P}s}$ of a generic acoustic path s, at a time $t_{0s}^{\pm} = \left(2s - \frac{1}{2}(3 \pm 1)\right) z_B$ are identical to fluctuation speed components existing in a time t=0 s in a location $-|\mathbf{u}_\infty|\left\{t_{0s}^{\pm} + \left[2s - \frac{1}{2}(3 \pm 1)\right] z_B\right\}$ backwards in the $-\mathbf{e}_{W1}$ direction.

5 Turbulent wind speed field in the atmosphere

Considering Eq. (26) in the Fourier–Stieldjes expression for turbulent wind speed given in Eq. (3), it is possible to obtain the expressions for the fluctuation components of wind speed vector $\mathbf{u}(\mathbf{x},\mathrm{t})$, experienced by the pulses travelling in both senses ± along the acoustic path $\mathbf{e}_{\mathbf{P}s}$ as follows

$$\hat{U}_{Wjs}^{\pm} = \hat{U}_{Wjs}^{\pm}\left(\mathbf{X}, \mathrm{X}_{\mathrm{Ps}}, l_{Ps}\mathrm{k}, P, M_\infty, c_{sj}^{PW}, s, Z_B\right) = \frac{1}{|\mathbf{u}_\infty|}\int_{-\infty}^{\infty} \exp\left\{ il_{Ps}\mathbf{k}\left[\begin{array}{c} \mathrm{X} + \mathrm{X}_{\mathrm{Ps}} + Pe_{\mathrm{Ps}} - \\ \left[\frac{M_\infty}{1 \pm c_{s1}^{PW} M_\infty}\left(\frac{1}{2} \pm P\right) + \left(2s - \frac{1}{2}(3 \pm 1)\right) Z_B\right] \mathbf{e}_{\mathrm{W1}} \end{array}\right]\right\} \mathrm{d}\Psi_j(\mathbf{k}, t) \tag{28}$$

Equation (24) represents the ± travelling pulse-referenced average of the dimensionless perturbation wind speed flow. Total flying times given by Eqs. (17) are introduced in Eq. (15) giving rise to

$$\begin{aligned} &U_{Ps}^{M}\left(\mathbf{X}, \mathbf{X}_{\mathrm{Ps}}, c_{sj}^{PW}, M_\infty\right) \\ &= c_{s1}^{PW} + \frac{1}{2}\left[\varepsilon F_s^{+}\left(\mathbf{X}, \mathbf{X}_{\mathrm{Ps}}, c_{sj}^{PW}, M_\infty\right) + \varepsilon F_s^{-}\left(\mathbf{X}, \mathbf{X}_{\mathrm{Ps}}, c_{sj}^{PW}, M_\infty\right)\right] \end{aligned} \tag{25}$$

which is the expression of the dimensionless measured wind speed component along the acoustic path $\mathbf{e}_{\mathbf{P}s}$.

Taylor's hypothesis of frozen turbulence can be applied to the expression of dimensionless wind speed fluctuation components path $\mathbf{e}_{\mathbf{P}s}$, $_{Wj}$,

$$\begin{aligned} &\hat{U}_{Wjs}^{\pm}\left[\mathbf{X}+\mathbf{X}_{\mathrm{Ps}} + Pe_{Ps}, T_{0s}^{\pm}\left(P, c_{s1}^{PW}, M_\infty\right)\right] \\ &= \hat{U}_{Wjs}^{\pm}\left\{ l_{Ps}\left[\begin{array}{c} \mathbf{X}+\mathbf{X}_{\mathrm{Ps}} + \mathrm{P}\mathbf{e}_{\mathrm{Ps}} - \\ \left[T_{0s}^{\pm}\left(P, c_{s1}^{PW}, M_\infty\right) + \left(2s - \frac{1}{2}(3 \pm 1)\right) Z_B\right] \mathbf{e}_{\mathrm{W1}} \end{array}\right]\right\} \end{aligned} \tag{26}$$

The last terms take into account the existence of a time delay Z_B between successive pulse firings, the initial times for the six pulse firings: T=0 (s=1+), T=Z_B (s=1–),···, T=5Z_B (s=3–) respectively. The elapsed time

Equation (24) can be rewritten in a more appropriate way

$$\begin{aligned} &\varepsilon F_s^{\pm}\left(\mathbf{X}, \mathbf{X}_{\mathbf{P}s}, l_{\mathrm{p}s}\mathbf{k}, M_\infty, c_{sj}^{PW}, s, Z_B\right) \\ &= \int_{-\frac{1}{2}}^{\frac{1}{2}} c_{sj}^{PW} \hat{U}_{Wjs}^{\pm}\left(\mathbf{X}, \mathbf{X}_{\mathbf{P}s}, l_{Ps}\mathrm{k}, M_\infty, c_{sj}^{PW}, s, Z_B\right) \mathrm{d}P \end{aligned} \tag{29}$$

After introducing Eq. (28) in Eq. (29), the perturbation terms $\varepsilon F_s^{\pm}$ are obtained

$$\begin{aligned} \varepsilon F_s^{\pm} = &\frac{1}{|\mathbf{u}_\infty|}\int_{-\infty}^{\infty} c_{sj}^{PW} \exp(i\mathbf{k}\mathbf{x}) G_s^{\pm}\left(\mathbf{X}_{\mathbf{P}s}, l_{Ps}\mathbf{k}, P, M_\infty, c_{s1}^{PW}, s, Z_B\right) \\ &\times \mathrm{d}\Psi_j(\mathrm{k}, t) \end{aligned} \tag{30}$$

where functions $G_s^{\pm}$ are defined by

$$\begin{aligned} G_s^{\pm} = \int_{-\frac{1}{2}}^{\frac{1}{2}} \exp\Bigg\{ &il_{Ps}\mathbf{k}\mathbf{X}_{\mathrm{Ps}} + il_{Ps}\mathbf{k}\mathrm{e}_{\mathrm{Ps}}P \\ &- i\left[\begin{array}{c} \frac{M_\infty}{1 \pm c_{s1}^{PW} M_\infty}\left(\frac{1}{2} \pm P\right) + \\ \left(2s - \frac{1}{2}(3 \pm 1) Z_B\right) \end{array}\right] k_{w1} l_{Ps} \Bigg\} \mathrm{d}P \end{aligned} \tag{31}$$

The integral expression in Eq. (31) can be solved to obtain

$$G_s^{\pm} = \exp\left[\begin{array}{l} il_{Ps}\mathbf{k}\mathbf{X}_{Ps} - \\ i\frac{1}{2}\frac{M_\infty k_{W1} l_{Ps}}{1 \pm c_{s1}^{PW} M_\infty} - \\ i\left(2s - \frac{1}{2}(3 \pm 1)\right) Z_B k_{W1} l_{Ps} \end{array}\right] \times \frac{\sin\left[\frac{1}{2}\left(l_{Ps}\mathbf{k}\mathbf{e}_{Ps} \mp \frac{M_\infty k_{W1} l_{Ps}}{1 \pm c_{s1}^{PW} M_\infty}\right)\right]}{\frac{1}{2}\left(l_{Ps}\mathbf{k}\mathbf{e}_{Ps} \mp \frac{M_\infty k_{W1} l_{Ps}}{1 \pm c_{s1}^{PW} M_\infty}\right)} \tag{32}$$

6 Measurement of the spectral density tensor

The measured wind speed vector in Wind system can be calculated from the measured components along each acoustic path by using the appropriate component transformation matrix

$$\mathbf{u}|_{\mathrm{SRV}} = \left[\mathbf{C}^{PW}\right]^{-1} \mathbf{u}_{\mathbf{P}}^{\mathbf{M}} \tag{33}$$

Conversely, the measured component of wind speed vector along each path is given by

$$u_{Ps}^{M} = |\mathbf{u}_\infty| \left[c_{s1}^{PW} + \frac{1}{2|\mathbf{u}_\infty|} c_{sj}^{PW} \int_{-\infty}^{\infty} \left(G_s^{+} + G_s^{-}\right) \exp(i\mathbf{k}\mathbf{x}) \mathrm{d}\Psi_j(\mathbf{k}, t)\right] \tag{34}$$

Considering Eq. (34), Eq. (33) gives rise to

$$\mathbf{u}^{\mathbf{M}}\big|_{\mathrm{WRS}} = |\mathbf{u}_\infty| \begin{Bmatrix} 1 \\ 0 \\ 0 \end{Bmatrix} + \left[\mathbf{C}^{WP}\right] \begin{Bmatrix} c_{11}^{PW} q_{11} + c_{12}^{PW} q_{12} + c_{13}^{PW} q_{13} \\ c_{21}^{PW} q_{21} + c_{22}^{PW} q_{22} + c_{23}^{PW} q_{23} \\ c_{31}^{PW} q_{31} + c_{32}^{PW} q_{32} + c_{33}^{PW} q_{33} \end{Bmatrix} \tag{35}$$

where

$$q_{sj} = \frac{1}{2} \int_{-\infty}^{\infty} \left(G_s^{+} + G_s^{-}\right) \exp(i\mathbf{k}\mathbf{x}) \mathrm{d}\Psi_j(\mathbf{k}, t) \tag{36}$$

and $\left[\mathbf{C}^{WP}\right] = \left[\mathbf{C}^{PW}\right]^{-1}$.

From Eq. (35), it is possible to extract the measured turbulent component of wind speed vector as follows

$$\widehat{\mathbf{u}}^{\mathbf{M}} = \left[\mathbf{C}^{WP}\right] \begin{Bmatrix} c_{11}^{PW} q_{11} + c_{12}^{PW} q_{12} + c_{13}^{PW} q_{13} \\ c_{21}^{PW} q_{21} + c_{22}^{PW} q_{22} + c_{23}^{PW} q_{23} \\ c_{31}^{PW} q_{31} + c_{32}^{PW} q_{32} + c_{33}^{PW} q_{33} \end{Bmatrix} \tag{37}$$

The fluctuation component of the wind speed vector, as measured by the sonic anemometer, can be expressed by means of a Fourier–Stieldjes expression, similar to Eq. (3), which describes the turbulent wind speed field

$$\widehat{u}_{Wj}^{M}(\mathbf{x}, t) = \int_{-\infty}^{\infty} \exp(i\mathbf{k}\mathbf{x}) \mathrm{d}\Psi_j^{M}(\mathbf{k}, t) \tag{38}$$

The comparison between Eqs. (37) and (38) gives rise to

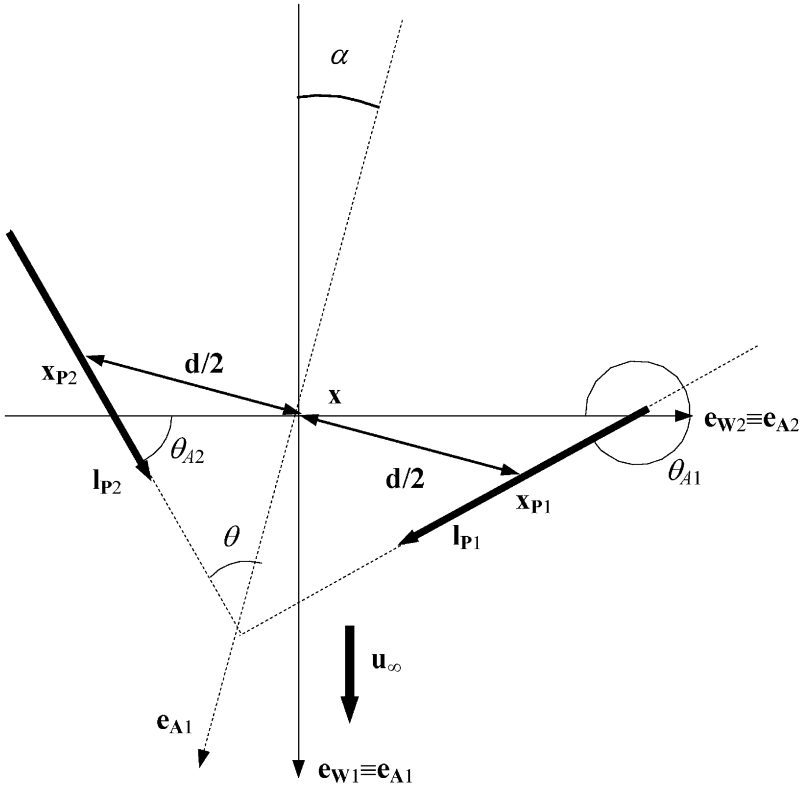

Fig. 3. Generic geometry of Kaimal's two-path sonic model. In the case analyzed, d/l=0.6, θ=60° and α=0° are redundant but are kept to facilitate the comparison with the results in Kaimal et al. (1968). For convenience in this case $\mathbf{e}_{Wj} \equiv \mathbf{e}_{Aa}$, j=a=1,2

$$\widehat{u}_{Wj}^{M}(\mathbf{x},t) = \int_{-\infty}^{\infty} \exp(i\mathbf{kx})\mathrm{d}\Psi_j^M(\mathbf{k},t) = c_{js}^{WP}c_{sr}^{PW}\int_{-\infty}^{\infty} Q_s \exp(i\mathbf{kx})\mathrm{d}\Psi_r(\mathbf{k},t) \quad (39)$$

Finally, Eq. (38) can be written for the measured spectral velocity tensor as follows

$$\Phi_{jt}^{M} = \overline{\mathrm{d}\Psi_j^M\left[\mathrm{d}\Psi_t^M\right]^*} = \overline{c_{js}^{WP}c_{sr}^{PW}Q_s\mathrm{d}\Psi_r\left[c_{tp}^{WP}c_{pm}^{PW}Q_p\mathrm{d}\Psi_m\right]^*} = c_{js}^{WP}c_{sr}^{PW}c_{tp}^{WP}c_{pm}^{PW}Q_sQ_p^*\Phi_{rm} \quad (40)$$

Equation (40) indicates that each component of the measured spectral velocity tensor, Φ_{jt}^{M} depends on all the components of the spectral velocity tensor, Φ_{rm}. Additionally, it is possible to establish a dependence on geometric parameters of the sensor, such as the midpoints of the acoustic paths, $\mathbf{x}_{Ps}$ and the acoustic path vectors $l_{Ps}\mathbf{e}_{Ps}$. Z_B appears as a parameter as well as Mach number, M_∞, incidence angles of mean wind vector θ_{AW} and γ_{AW}, and the ratio between the estimation of integral length scale and the length of the path, λ. It is important to remark that the influence of M_∞ and Z_B is a direct consequence of the main hypothesis of this paper, which states that flow variations during pulse travel sequence influence the measurement (Cuerva and Sanz-Andrés 2000).

The spectral density functions measured at one point are given by

$$F_{jt}^{M}(\mathbf{x}_{Ps},\mathbf{I}_{Ps},Z_B,M_\infty,k_{W1}) = \int_{-\infty}^{\infty}\int_{-\infty}^{\infty}\Phi_{jt}^{M}(\mathbf{x}_{Ps},\mathbf{I}_{Ps},Z_B,M_\infty,k_{W1},k_{W2},k_{W3})\mathrm{d}k_{W2}\mathrm{d}k_{W3} \quad (41)$$

7 Results of the new model applied to a two-path sonic anemometer

In 1968, Kaimal presented results for the relation of the measured spectral density function and the theoretical one for a two-path sonic anemometer configuration (see Fig. 3). Kaimal obtained such results by applying his theory of instantaneous line average for the pulse transmissions. In this section, the effect of Mach number, M_∞, and time delay between consecutive pulses, Z_B, are analyzed using Kaimal's case as a reference (Kaimal et al. 1968).

In Fig. 4, a varying Z_B gives rise to an amplification region for certain interval of parameter Z_B in the measurement of longitudinal spectral density, F_{11} ($R_{11}>R_{11}|_{ZB=0,\ M\infty=0}$). In the case of M_∞=0, a semi-interval $Z_B\in$[0.08,0.245] presents absolute amplification in the measurement of F_{11} ($R_{11}>1$). For values of Z_B greater than certain value of parameter Z_B ($Z_B>Z_B|_{R11MAX}$) the attenuation in the measurement of F_{11} becomes more intense. Increasing M_∞ gives rise to decreasing values of R_{11} indicating more intense attenuation in the measurement of F_{11}. For larger values of Z_B, the decreasing trend of R_{11} as M_∞ increases becomes inverted.

In this two-path case the trends described in Cuerva and Sanz-Andrés (2000) are complemented. In Cuerva and Sanz-Andrés (2000), a strong variation in R_{11} was found vs $k_{W1}l$ for varying values Z_B. In this case, for a given value of parameter $k_{W1}l$, a significant dependence on the delay between consecutive pulses shots Z_B is found, which may lead to amplifications or attenuations in the measurement. The dependence on M_∞ is reproduced as in (Cuerva and Sanz-Andrés 2000). In the first term, this dependence is less strong. Additionally, for a given value of $k_{W1}l$, the decreasing trend of R_{11} as M_∞ increases is inverted for large values of Z_B. A similar result for R_{11} is described in

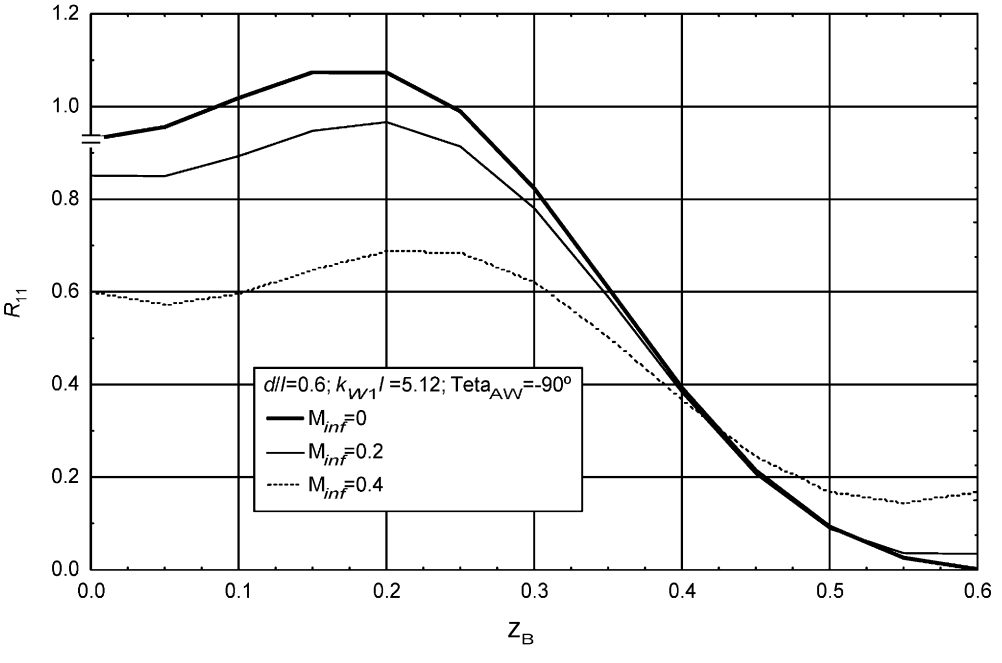

Fig. 4. Variation of the relation of longitudinal spectral components R_{11} vs dimensionless time delay between consecutive pulses shots, Z_B. $M_{inf} \equiv M_\infty$ is the Mach number of the incoming flow. d is the distance between path centers. $k_{W1}l$ is the longitudinal component of the wave number vector $\mathbf{k}$ multiplied by the path length, l. $Teta_{AW} \equiv \theta_{AW}$ is the incidence angle of mean wind speed vector in the plane $\mathbf{e}_{A1}\mathbf{e}_{A2}$. Mark at Z_B=0 (M_∞=0) represents the predicted value by Kaimal in instantaneous line-averaging conditions

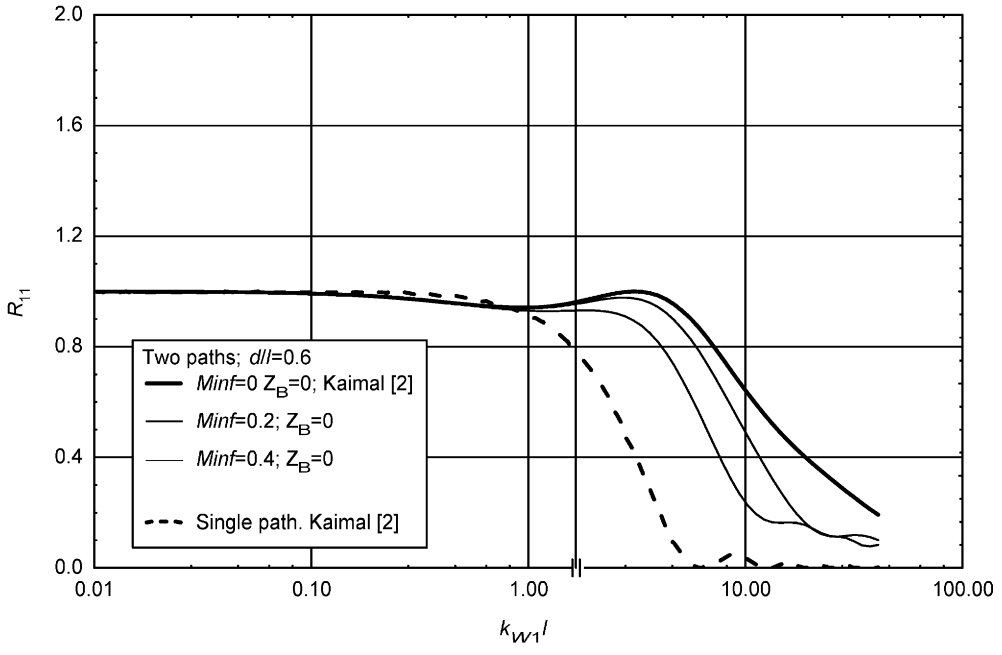

Fig. 5. Influence of Mach number $M_{\text{inf}} \equiv M_\infty$ in the relation of longitudinal spectral components R_{11}. d is the distance between path centers. $k_{W1}l$ is the longitudinal component of the wave number vector **k** multiplied by the path length, l

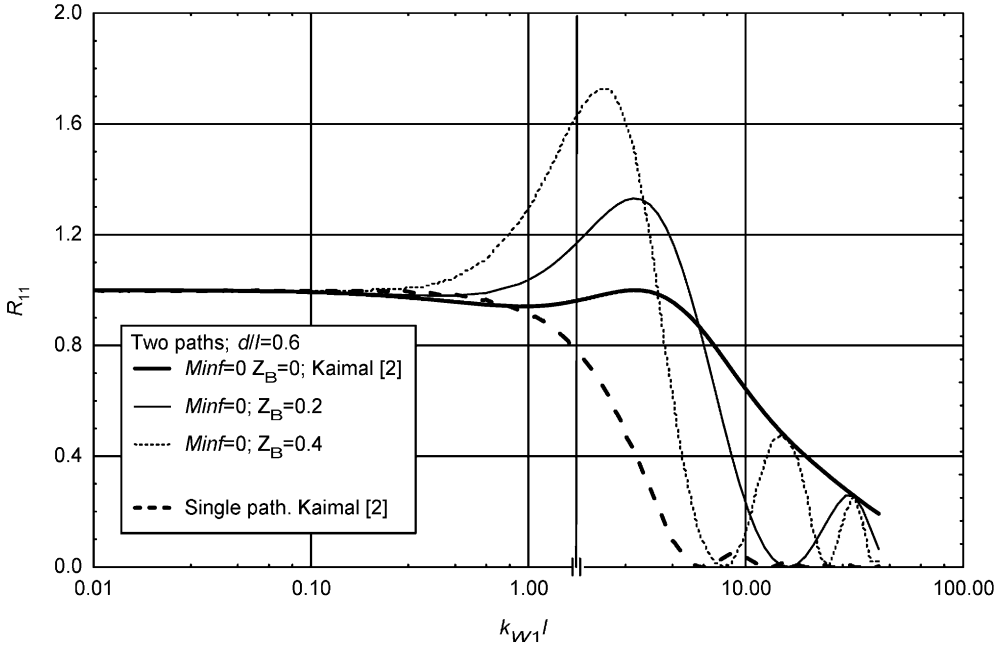

Fig. 6. Influence of dimensionless time delay between consecutive pulses shots, Z_B, in the relation of longitudinal Spectral components R_{11}. d is the distance between path centers. $k_{W1}l$ is the longitudinal component of the wave number vector k multiplied by the path length, l

Cuerva and Sanz-Andrés (2000) for Z_B=0 for large values of $k_{W1}l$.

Both the Mach number M_∞ and time delay between consecutive pulses, Z_B induce significant variations in function R_{11} with regard to Kaimal case, see Figs. 5 and 6 respectively. These variations are more intense than the ones induced by the dimensionless distance between acoustic path centers, presented in Kaimal et al. (1968). The complexity of geometry gives rise to a modification in the way the results are influenced by time delay between consecutive pulses. Cuerva and Sanz-Andrés (2000) described how R_{11} variations induced by $Z_B \neq 0$ do not lead, in any studied case, to R_{11} values greater than the value corresponding to the Kaimal case (M_∞=0, Z_B=0) for a one acoustic path configuration. However, Fig. 6 describes how, in a more complex geometry, large values of time delay give rise to amplification values for R_{11} larger than the corresponding values of Kaimal case for some intervals of $k_{W1}l$. These results were already anticipated for a given value of $k_{W1}l$ in Fig. 4. Kaimal et al. (1968) established the values $k_{W1}l$=1 and $k_{W1}d$=1 as limits for the influence of sonic measurement process in the determination of spectral density functions. However, the combination of $M_\infty \neq 0$ and $Z_B \neq 0$ gives

rise to variations of these limits. In Figs. 5. and 6, the limit value associated with the distance between center, $k_{W1}d$=1 leads to a limit value associated with the length of the acoustic paths $k_{W1}l$=1.66, since d/l=0.6. The values of the ratio of spectral components, R_{11}, are clearly different than unity, especially for $Z_B \neq 0$ (see Fig. 6). The perturbation effect of $M_\infty \neq 0$ is not that strong (Fig. 5).

A generalization of this result can be established by defining two new limits for a given configuration of sonic anemometer. These new limits can be defined as $k_{W1}l=C_l$ and $k_{W1}l=C_d$ for the effect of line averaging and distance between path mid points respectively. Hence, the lower longitudinal wave numbers for which the spectral density functions are remarkably influenced by the effect of finite path, l (line averaging), and distance between paths, d, as predicted by the new model, are $k_{W1}=C_l/l$ and $k_{W1}=C_d/d$ instead of $k_{W1}=1/l$ and $k_{W1}=1/d$ predicted by the instantaneous line-averaging model. An immediate consequence is that line-averaging effect and distance between paths effects cannot be treated independently from the other parameters that appear in the problem, since both, C_l and C_d depend on the geometry of the sensor, the operational process (sequence and time delay between consecutive pulses) and mean flow characteristics (Mach number and incidence angles of mean wind speed vector).

Normally C_l and C_d are lower than unity, so that, for a given sonic anemometer, the limit k_{W1} predicted by the new model is lower than the one predicted by Kaimal's instantaneous line-averaging model. This fact has required a revision of the validity of inertial sub-range formulation commented on by Kaimal et al. (1968) for the application of Kaimal's model.

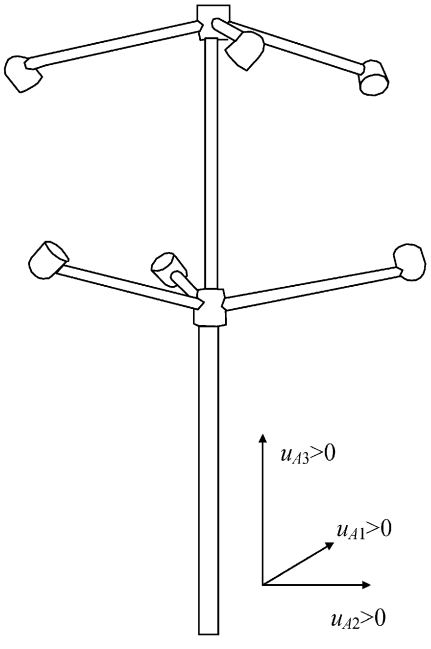

Fig. 7. Sketch of the METEK USA 1 sonic anemometer. Measured wind speed components u_{Aa} following x,y,z>0 are positive

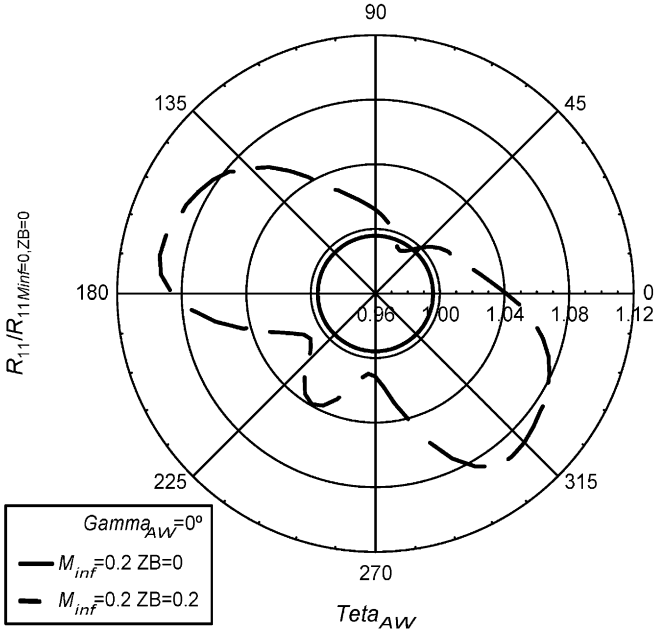

Fig. 8. Azimuthal variations in the ratio of spectral components R_{11} scaled with R_{11} for Mach number $M_{inf} \equiv M_\infty$=0 and dimensionless time delay between consecutive pulses shots, Z_B=0. $Gamma_{AW} \equiv \gamma_{AW}$, elevation angle of mean wind speed vector. $Teta_{AW} \equiv \gamma_{AW}$, azimuth angle of mean wind speed vector. METEK USA

Hence, the use of Eq. (6) for the function $E(k)$ is directly linked with the existence of the so defined inertial sub-range of turbulence (Kaimal et al. 1968) where, as is quite well known (Lumley and Panofsky 1964), neither production nor energy dissipation occurs. The wavenumbers that define the inertial sub-range are given by

$$\frac{1}{l_W} << k_{W1} << \frac{1}{\eta} \tag{42}$$

where η is Kolmogorof's length, typically of order 0.001 m (Lumley and Panofsky 1964). For usual sensor design and normal atmospheric situations this is $l<<l_W$ (more specifically in this work $\lambda=l_W/l$=100). In this work, Kaimal's limit for measurement distortion, $k_{W1}=1/l$, has been reviewed, the new limit being defined as $k_{W1}l_{CRIT}=C_l$. For a given path length, the influence threshold value provided by the new model is $k_{W1}=C_l/l<1/l$, even though this relation exists, the results show that $k_{W1}=C_l/l>>1/l_W$ and therefore the wavenumbers for which the sonic anemometer process has an important influence are enough larger than the minimum wavenumber of applicability of inertial sub-range formulation ($1/l_W$). The reasoning presented by Kaimal et al. (1968) for the upper limit of the inertial sub-range still remains applicable. For the upper region of inertial sub-range, k_{W1} values are beyond the operations limits (Lumley and Panofsky 1964) of even the latest generation sonic anemometers (Cuerva 2001) (sampling rate≈100 Hz), i.e.,

using the frozen turbulence hypothesis, a wave-number $k_{W1}=1/\eta\approx1000\ m^{-1}$ for $|u_\infty|=10$ m/s gives rise to a characteristic frequency of about 1600 Hz, quite beyond the maximum sampling performances of modern sonic anemometers. This reasoning evidences the applicability of Kármán's turbulence formulation in the general model of a sonic anemometer measuring process.

8
Influence of wind direction

The conclusions established for the case of a two-path configuration can be applied to a generalized three-path sonic anemometer configuration (Fig. 7). Specifically, in this section, the influence of the incidence angles of mean wind speed vector is analyzed. In Kaimal et al. (1968), this influence was established for the two-path sonic anemometer configuration already mentioned. In his work, Kaimal presented important differences in the determination of R_{11} and R_{22} for values $k_{W1}l>1$. When parameters $M_\infty>0$ and $Z_B>0$ are considered, the influence of wind speed direction, relative to the sensor can become intensified, even for $k_{W1}l\approx1$.

In Fig. 8, the ratio of function R_{11} ($M_\infty=0.2$ and $Z_B=0$, 0.2) over R_{11} (Kaimal, $M_\infty=0$ and $Z_B=0$) is presented for $k_{W1}l=1$ and a wind speed incidence angle $\theta_{AW}\in[0°,360°]$. It must be remarked that a variation in θ_{AW} for $\gamma_{AW}=0°$ (as is the case) is fully equivalent to a variation in wind direction in a real field test for a perfectly horizontally levelled sensor. The geometry used in this computational test is shown in Fig. 7.

Figure 8 shows a clear example of the influence of Mach number and time delay between consecutive pulses. For the case $M_\infty=0.2$ and $Z_B=0$, the ratio of R_{11} functions is lower than unity, keeping undistorted the triple symmetry associated with the three paths equally spaced in the horizontal plane. Hence, the influence of Mach number, for this wavenumber, is a slight additional attenuation related to the instantaneous line-averaging analysis ($M_\infty=0$ and $Z_B=0$). Conversely, the case $M_\infty=0.2$ and $Z_B=0.2$ shows the strongest influence of even such a small time delay (for a given typical mean wind speed $|\mathbf{u}\infty|=10$ m/s and an usual acoustic path length, $l=0.1$, dimensionless time delay $Z_B=0.2$ gives rise to dimensional time delay of $z_B=0.002$; values of this order are normal in sonic anemometry). The effect of time delay gives rise to important general extra amplifications in the measurement of the longitudinal spectral density function related to the values predicted by the instantaneous line-averaging model. Maximum extra amplifications around 10% are found for certain incidence angles θ_{AW} (equivalent to wind direction). Additionally, the Z_B effect leads to a significant distortion of symmetry in the measurement associated with the path geometry already mentioned. This azimuthal distortion of symmetry could be interpreted (from uncorrected real measurements) as an additional different energy content of turbulence for the analyzed wavenumber, depending on the wind direction considered, but in fact it is due to a measurement error of the sensor.

9
Conclusions

Taking into account time variations in flow speed during the sequence of pulses in the mathematical model of a multiple-path sonic anemometer (hypothesis already applied by the authors to a single-path configuration), along with the geometry of sensors and the incidence angles of mean wind speed vector, gives rise to additional significant wave-number-dependent errors not considered up to now by instantaneous line-averaging models.

Consideration of the new model points to the necessity of a generalization of Kaimal's limits $k_{W1}=1/l$ and $k_{W1}=1/d$. The existence of a time delay between consecutive pulses, fundamentally, and the evolution of turbulent speed field during the transmission of a pulse, represented by a Mach number greater than zero give rise to two new limits (linked to path length and path separation) for the influence of sonic anemometer process on the measurement of turbulence. These new limits are $k_{W1}=C_l/l$ and $k_{W1}=C_d/d$ respectively, where both, C_l and C_d depend on the time delay between consecutive pulses, Mach number, geometry of the specific sensor and the incidence angles of the mean wind speed vector.

The new model evidences that time variations during the sequence of pulses that give rise to a measured value of wind speed vector (neglect by instantaneous averaging models) lead to important additional corrections of turbulence measurement (relative to the corrections given by instantaneous averaging models).

It must be remarked that this paper deals exclusively with the modeling of pulse sequences, which is one part (although the most characteristic) of the complete process of sonic anemometer measurement. The joint analysis of this part with the discrete treatment of single sequences will be considered in future work.

References

Batchelor GK (1952) The theory of homogeneous turbulence. Cambridge Monographs on Mechanics and Applied Mathematics

Cuerva A (2001) New models in sonic anemometry. Thesis. Universidad Politécnica de Madrid, ETSI, Aeronauticos, Instituto Universitario Ignacio DaRiva, Madrid

Cuerva A, Sanz-Andrés A (1999) Steps to reach a safe scenario with sonic anemometers as standard sensor for wind measurements in wind energy. European Wind Energy Conference, Risø, EWEA and WIP, Nice. James & James, London, pp 649–652

Cuerva A, Sanz-Andrés A (2000) On sonic anemometer measurement theory. J Wind Eng Ind Aerodyn 88:25–55

Cuerva A, Sanz-Andrés A, Benzdenejnykh N, Perales JM (1998) Assessment of performances of ultrasonic anemometers as one step ahead in wind measurements of energy production of a wind turbine. European Wind Energy Conference, EWEC. R. Watson, Dublin, pp 418–421

Henjes K, Taylor PK, Yelland MJ (1999) Effect of pulse averaging on sonic anemometer spectra. J Atmos Oceanic Technol 16:181–184

Kaimal JC (1978) Sonic anemometer measurement of atmospheric turbulence. In: Dynamic flow conference. Pergamon Press, Oxford, pp 551–565

Kaimal JC, Wyngaard J, Haugen DA (1968) Deriving power spectra from a three-component sonic anemometer. J Appl Meteorol 7:827–837

Kato N, Ohkuma T, Kim JR, Marukawa H, Niihori Y (1992) Full scale measurements of wind velocity in two urban areas using an ultrasonic anemometer. J Wind Eng Ind Aerodyn 41–44:67–68

Lumley JL, Panofsky HA (1964) The structure of atmospheric turbulence. Interscience, New York

Mann J (1994) Models in micrometeorology. Risø, Roskilde, Denmark

Von Kármán T (1958) Progress in the statistical theory of turbulence. Proc Nat Acad Sci USA 34:530–539